



**HAL**  
open science

## Hydrodynamic performance evaluation of a new hydrofoil design for marine current turbines

Mourad Nachtane, Mostapha Tarfaoui, D. Saifaoui, M. Rouway

### ► To cite this version:

Mourad Nachtane, Mostapha Tarfaoui, D. Saifaoui, M. Rouway. Hydrodynamic performance evaluation of a new hydrofoil design for marine current turbines. 1st International Conference on Renewable Energy and Applications, ICREA 2019, Dec 2019, Casablanca, Morocco. pp.889-898, 10.1016/j.matpr.2020.04.346 . hal-02995497

**HAL Id: hal-02995497**

**<https://ensta-bretagne.hal.science/hal-02995497>**

Submitted on 17 Jun 2021

**HAL** is a multi-disciplinary open access archive for the deposit and dissemination of scientific research documents, whether they are published or not. The documents may come from teaching and research institutions in France or abroad, or from public or private research centers.

L'archive ouverte pluridisciplinaire **HAL**, est destinée au dépôt et à la diffusion de documents scientifiques de niveau recherche, publiés ou non, émanant des établissements d'enseignement et de recherche français ou étrangers, des laboratoires publics ou privés.



Distributed under a Creative Commons Attribution 4.0 International License

# Hydrodynamic performance evaluation of a new hydrofoil design for marine current turbines

M. Nachtane <sup>a,\*</sup>, M. Tarfaoui <sup>b</sup>, D. Saifaoui <sup>c</sup>, M. Rouway <sup>c,d</sup>

<sup>a</sup> *Institute of Mechanical Engineering (I2M), UMR CNRS 5295, University of Bordeaux, 33405 Talence Cedex, France*

<sup>b</sup> *ENSTA Bretagne, IRDL - UMR CNRS 6027, F-29200 Brest, France*

<sup>c</sup> *Laboratory for Renewable Energy and Dynamic Systems, FSAC - UH2C, Morocco*

<sup>d</sup> *REMTEX Laboratory, Higher School of Textile and Clothing Industries (ESITH), Casablanca, Morocco*

Tidal energy has clear potential in producing large amounts of energy as the world's capacity exceeds 120 GW. Despite being one of the oldest renewable energy sources exploited by man, the technology is still in its pre-commercialisation stage and so lags behind other renewable sources such as wind and geothermal energy in terms of development and energy produced. One of the emerging energy extraction technologies in the tidal energy field is the Horizontal Axis Hydrokinetic Turbine (HAHT) which harness tidal stream energy the same way Horizontal Axis Wind Turbine (HAWT) extract energy from the wind. While HAHT has been the topic of many researches over the past decade, design of hydrofoils plays a vital role in increasing the structural strength of the blade and maximizing the output of the marine current turbines. In this context, a numerical investigation is conducted in this research in which new hydrofoil for marine current turbines underwater conditions was designed and evaluated. The turbine blade is designed using XFLR5 code and QBlade which is a Blade-Element Momentum solver with a blade design feature. Then, the hydrodynamic performance of hydrofoil was tested using Computational Fluid Dynamics (CFD) consisting of lift and drag coefficients, and velocities distribution. The results showed that the new design of the hydrofoil of marine current turbine blade maintained a  $C_{Power}$  value of 50% more from normal range at the TSR 5 to 9 and 51% more at TSR = 6,5 in the performance curve.

## 1. Introduction

Currently, the issue of global warming is becoming a one of the vital concerns for the mankind and rapidly becoming a huge distress in social media because of its alarming negative impact on the environment [1–4]. Fortunately, the world has come together to fight this problem by increasing the use of renewable energies for their energy production and this led to the development of a

new sector of energy in which ocean energy is used for energy production because oceans cover 70% of the world's surface [5,6]. Ocean energy technologies exist in different forms: waves, currents, thermal gradients, salinity gradients, tides, and the wind [7–10] therefore, renewable marine energies are appear to be a tremendous opportunity to give rise to a new industrial sector at the crossroads of blue and green growth and to create sustainable jobs [11]. Numerous research and development initiatives had been taken by several academic institutions in different regions such as the United Kingdom, the United States, Canada, and Norway etc. to accelerate the energy transition to renewable energy sources, as shown in Figs. 1 and 2 [12] and also develop the research in composite behavior in tidal turbine of the marine energy [13–17].

Various investigations had been conducted to develop an appropriate blade section for the marine current turbine. The

*Abbreviations:* HAHT, Horizontal Axis Hydrokinetic Turbine; CFD, Computational Fluid Dynamics;  $C_{Power}$ , Coefficient of power; TSR, Tip speed ratio; TCTs, Tidal current turbine; EMEC, European Center for Marine Energy; NACA, National Advisory Committee for Aeronautics; BEM, Boundary Element Method;  $C_L$ , Coefficient of lift;  $C_D$ , Coefficient of Drag; AOA, Angle of Attack;  $C_{p_{min}}$ , Coefficient of pressure.

\* Corresponding author.

E-mail address: mourad.nachtane@u-bordeaux.fr (M. Nachtane).

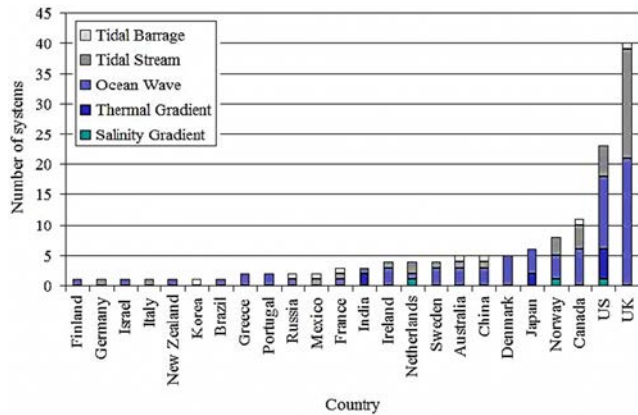


Fig. 1. Country share in renewable marine energy system development.

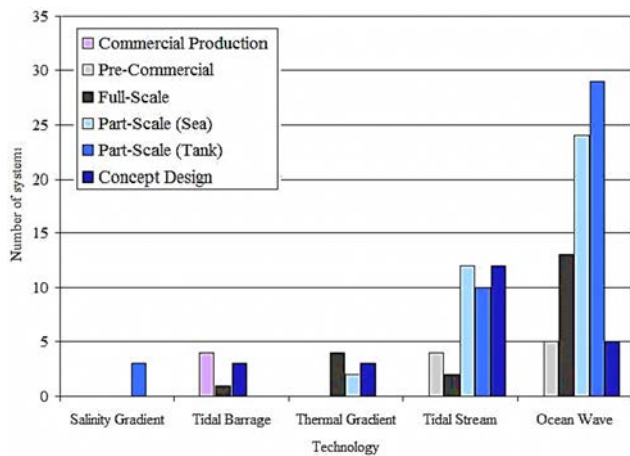


Fig. 2. Technology maturity of various ocean energy conversion schemes.

principal purpose of the new blade design was to improve the coefficient of lift and reduce the coefficient of drag and the coefficient of pitching moment. Ahmed [18] performed an overall evaluation of the structure of the blade to utilize it in TCTs. Goundar et al. [19] studied the HF10XX series of the blade to design a 3-bladed horizontal axis tidal current turbine rotor of 10 m diameter (HF present the abbreviation of the hydrofoil). They designed the blade using new hydrofoil design, with different thickness of each hydrofoil with respective to the position and achieved the maximum power of 150 kW and maximum efficiency of 47.5% at the 2 m/s current rate. Lawson and Sale [20] used a NACA 63-series blade to model a HAHT (Horizontal Axis Hydrokinetic Turbine) rotor of 20 m diameter because the coefficient of pressure was big enough for this hydrofoil to ensure good resistant to cavitation. Grasso [21] designed two novel hydrofoils, G-hydra-A and G-hydra-B using an algorithm of sequential quadratic programming (SQP) and these hydrofoils showed excellent performance, similar to DU96-W-180 and NACA 4418 blade parts. Batten et al. [22] used a NACA 63-8xx series to predict horizontal axis rotor characteristics and described the cavitation experiment for the NACA series (63-815 and 63-215). Molland et al. [23] assessed lift and drag feature of NACA 6615, 63-815 and 63-215 experimentally using cavitation tunnel and numerically using numerical codes and showed that the hydrofoil with high lift coefficient and high camber resulted in limited cavitation.

Marine currents could result in a significant and predictable source of renewable energy [24]. The rotor blades were first made

of steel which led to various problems such as expensive manufacturing processes, difficulties in handling due to their heavyweight and deteriorating marine environment, in addition, adequate strength and stiffness were the critical requirements for the marine current turbine. These requirements could only be fulfilled using high performance reinforce materials such as composites because of their weight, efficiency, endurance, and cost [25–27].

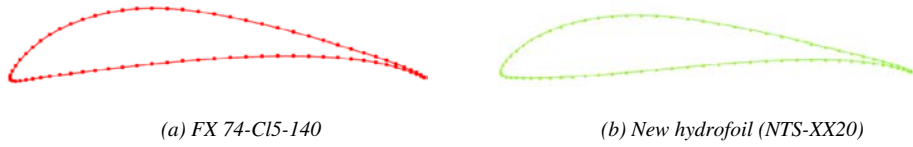
In order to enhance the turbine energy output and provide enough durability to the blade structure, hydrofoils must be rightly designed [28]. The requirements of HATCT conception, which are mostly, associated with problems such as mass gain, fouling resistance, corrosion resistance, manufacturing methods and coating technology according to Nachtane et al. [29], the future work will involve the use of composite materials because of their excellent mass/durability relations. This paper shows a new design of hydrofoil for Horizontal Axis Hydrokinetic Turbine. Hydrofoils were designed for various blade position; they are called as NTS-XX20. The hydrodynamic performance of the hydrofoils was presented. It was guaranteed that the designed hydrofoils with delayed cavitation while the required working conditions with the low profile and the drag the high maximum lift and the insensitive to roughness have been achieved. The features of the NTS-XX20 hydrofoils were linked with other frequently employed hydrofoils.

## 2. Hydrofoil selection

Generally, Computational fluid dynamic (CFD) is commonly used to do the performance analysis of a hydrofoil and in addition, Xfoil and XFLR5 are the tools frequently used for a 2D model of the hydrofoil which includes study of lift-coefficient ( $C_L$ ), drag coefficient ( $C_D$ ), and the pressure-coefficient ( $C_{pmin}$ ) [30]. However, when the required parameters are rightly set, with the same viscosity and Reynolds number, Xfoil/XFLR5 can also be utilized for design and analysis hydrofoil [29,31]. In this work, WORTMANN (FX74-CL5-140) airfoil, suited for low Reynolds number regime and high lift ability, was selected for analysis and a new hydrofoil was designed by changing the shape of WORTMANN to improve its hydrodynamic characteristics and to make it operate at the necessary requirement for hydrokinetic turbines. Hydrofoil was redesigned by interactive modification of geometric parameters such as Max thickness and camber, highpoint position, LE radius, TE thickness, camber line via geometry specification, camber line via loading change specification, flap deflection, and explicit contour geometry and then subjected it to computational analysis, Fig. 3. The Table 1 presents the differences between the two hydrofoils (FX 74-CL5-140 and NTS-XX20).

## 3. Qblade software validation

The software QBlade is developed as an open source framework for the simulation and design of wind turbines. QBlade utilizes the Blade Element Momentum (BEM) method for the simulation of horizontal axis and a Double Multiple Streamtube (DMS) algorithm for the simulation of vertical axis wind turbine performance. For the design of custom airfoils and the computation of airfoil lift and drag coefficient, polar the viscous-inviscid coupled panel method code XFLR5 is integrated within the graphical user interface of QBlade. The software XFLR5, with all its functionality, is integrated seamlessly into QBlade to generate two dimensional airfoil coordinates for blade design and airfoil lift and drag coefficients for turbine simulations, Fig. 4. In this context, XFLR5 codes show good correlation with the experimental results, in fact, a comparison of the performance of the XFLR5 with the experimental results is shown in Fig. 5. The correlation between the two plots is generally acceptable although an over prediction of QBlade's



(c) Hydrofoil Manufacture using Additive Manufacturing

Fig. 3. Design of new Hydrofoil (NTS-XX20).

**Table 1**  
Comparison between FX 74-CL5-140 and NTS-XX20.

Name	Thickness (%)	Camber (%)	Camber maximum position (%)	Points
FX 74-CL5-140	13.08	9.72	27.10	79
NTS-XX20	20	10	27.10	79

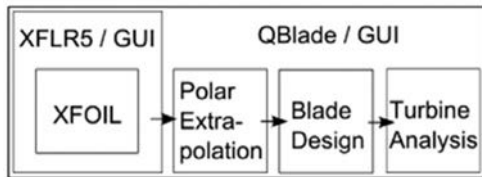


Fig. 4. Software modules inside Qblade.

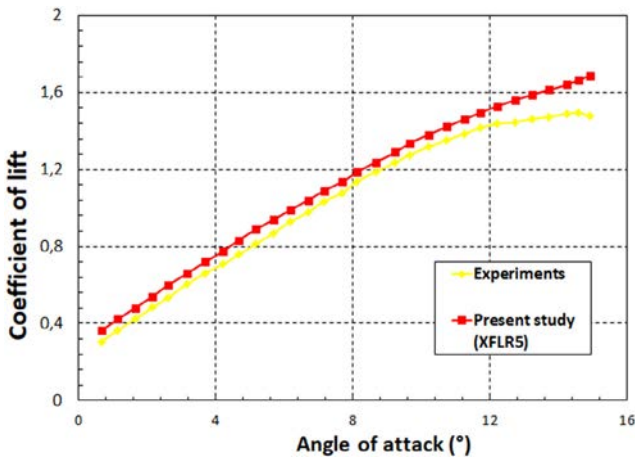


Fig. 5. Comparison of lift coefficients obtained by numerical results and experiments.

results can be observed for angles of attack greater than  $10^\circ$ . The flow after this point will be harder to predict because of flow separation and turbulence.

The next step was to test the blade element momentum (BEM) solver of QBlade. This was carried out by validating the results with the experimental data of Bahaj et al. [23]. The blade used in the experiment has a geometry composed of NACA 63-8xx foils with

NACA 63-824 at the root and NACA 63-812 at the tip. The rotor performance curves (CP vs TSR) in the reference were compared with the results of the QBlade simulations as shown in Fig. 6. The rotor was simulated for two pitch angles at  $20^\circ$  and  $25^\circ$  over a TSR range of 2–10. These pitch angles were chosen by the Bahaj group with the  $20^\circ$  pitch as the optimum pitch angle. As can be seen in the plot, there is satisfactory agreement between the two sets of data. The general trend of the experimental plot was captured by the QBlade simulation. There is some under prediction especially for low TSRs where higher AoA on the blade is expected, making the performance harder to predict because of possible flow separation. Overall, QBlade shows a good prediction of the rotor performance and is deemed acceptable to be used as a design tool.

NTS-XX20 in comparison to FX74-CL5-140 showed that it had greater  $C_L$ , lower  $C_D$ , and more thickness thus, providing more strength and durability to the blade structure, Figs. 7 and 8.

Tables 2 and 3 present percent differences at each region of coefficient of lift and drag. The Percentage Difference between

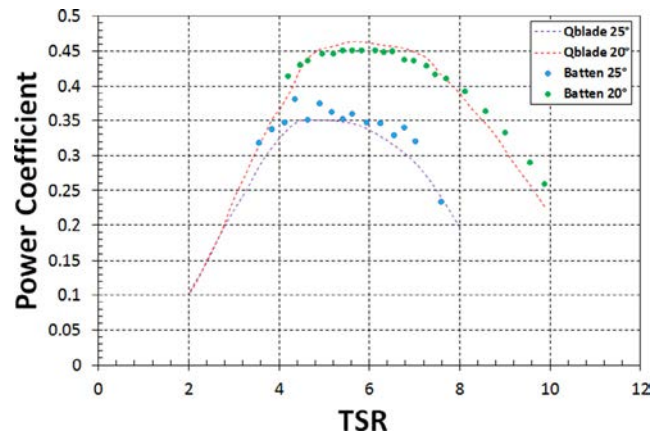


Fig. 6. Comparison of performance curves from the QBlade BEM results and experimental data for the Bahaj et al. [23].

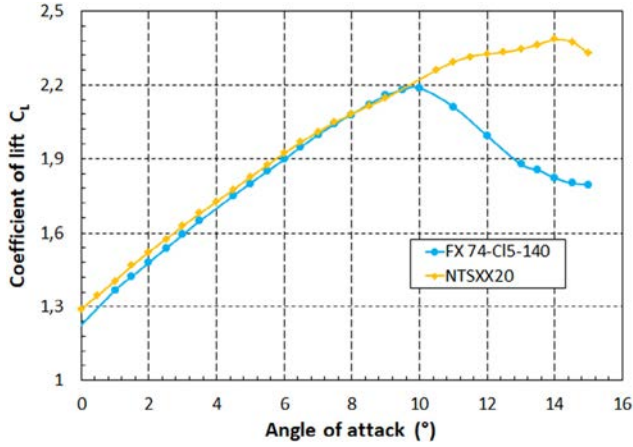


Fig. 7. Variation of the coefficient of lift for NTS-XX20 compared with FX74-CL5-140 at different AOA and  $Re = 2.10^6$ .

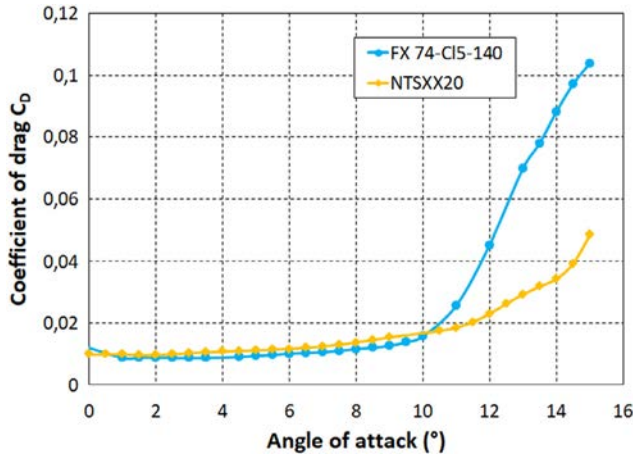


Fig. 8. Variation of the coefficient of drag for NTS-XX20 compared with FX74-CL5-140 at different AOA and  $Re = 2.10^6$ .

two curves (two hydrofoils) is given by equation (1) for lift coefficient and (2) for drag coefficient:

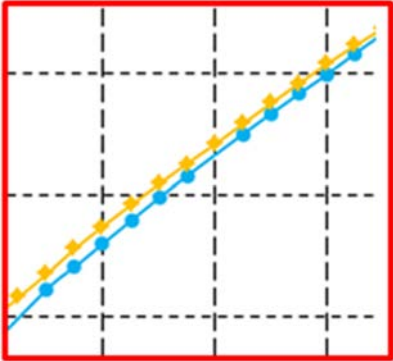
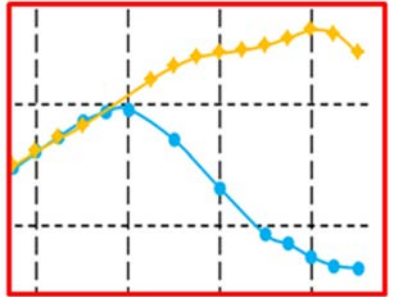
$$\frac{|C_{L1} - C_{L2}|}{\frac{(C_{L1} + C_{L2})}{2}} \times 100 \quad (1)$$

$$\frac{|C_{D1} - C_{D2}|}{\frac{(C_{D1} + C_{D2})}{2}} \times 100 \quad (2)$$

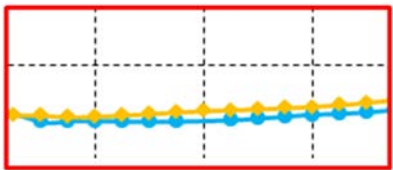
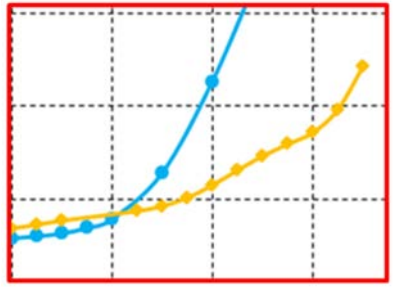
For more illustration, the pressure coefficient designed around hydrofoil is presented in Fig. 9 for the AOA  $13^\circ$ . The pressure built in the top surface for both hydrofoils diminishes quickly from leading to trailing edge but in the inferior side it grows. With the growing of relative thickness, coefficient of pressure reduces more gently in the upper surface but grows quickly in the lower surface. Pressure variance grows with growing hydrofoil thickness once linked superior and inferior surfaces. Though, with the growing relative thickness, the coefficient of drag also rises and the coefficient of lift growth is not proportionate to the thickness of hydrofoil. If coefficient of drag didn't grow with the thickness of hydrofoil, thick hydrofoil would have a greater coefficient of lift.

Growing thickness and the camber of hydrofoil growths, can be viewed the minimum coefficient of pressure  $C_{pmin}$  in Fig. 8, minimum  $C_{pmin}$  of FX74-CL5-140 at  $13^\circ$  AOA ( $\alpha$ ) is about  $-3,9$  and for NTS-XX20 it has augmented to about  $-3$ . This will restrict the

**Table 2**  
Percent differences at each region of lift coefficient.

Angle of attack	Region	The Percentage Difference
0–7°		12,82%
7,5–16°		15,11%

**Table 3**  
Percent differences at each region of coefficient of drag.

Angle of attack	Region	The Percentage Difference
0–7°		9,26%
7,5–16°		14,11%

cavitation phenomena; despite the missing zone in growing the force pressure is augmented as the  $C_{pmin}$  among lowest  $C_{pmin}$  and the transition region rises, later grew  $C_L$  and decreased  $C_D$  of the hydrofoil can be observed in Figs. 6 and 7.

Moreover, the it is important to ensure that the turbine rotor had higher torque ( $T$ ) and speed ( $\omega$ ) by confirming a good manufacturing design of the blade so it can result in higher power generation ( $W$ ), see Eq. (3).

$$W = T \times \omega \quad (3)$$

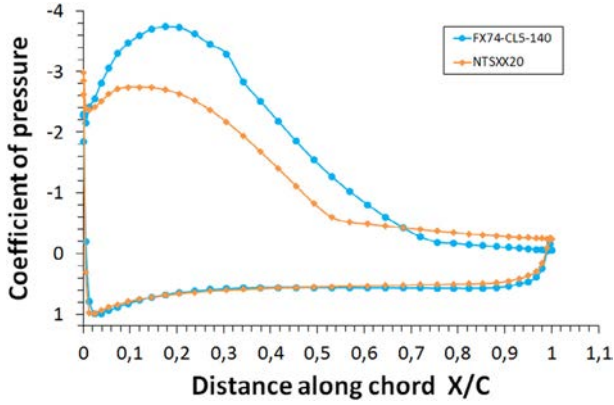


Fig. 9. Pressure coefficient distribution of NTS-XX20 and FX74-CL5-140 at  $\alpha = 13^\circ$  and  $Re = 2.10^6$ .

Torque and angular speed of the rotor were obtained by hydrofoil lift forces, Fig. 10. Lift force was generated by the change in pressures ( $\Delta P$ , Eq. (3)) and this change in pressures was produced on the surface of hydrofoils which was dependent on the parameters such as fluid density, airfoil surface profile and the hydrofoil angle of attack  $\alpha$  (Eq. (4)) [32,33].

$$\Delta P = P_{upper\ surface} - P_{bottom\ surface} \quad (4)$$

QBlade's BEM code was used to simulate the hydrodynamic performance curve of the marine current turbine under the operating conditions of incoming water velocity of 2 m/s over a TSR range from 1 to 10. The XFLR function of QBlade and the 360° polar Montgomery extrapolated method were used to find the lift and drag coefficient for each hydrofoil sections, Fig. 11. Data acquired from XFLR was implemented in the BEM function of Qblade using the created design of the marine current turbine.

Fig. 12 shows that the performance curve of the designed marine current turbine blade maintained a  $C_{Power}$  value at 50% at  $TSR = 6.5$ . The results show that the new hydrofoil design is better.

#### 4. CFD simulation of hydrofoils

The CFD simulations of new hydrofoil as 2D model were carried out using the Abaqus FE code and it also required the definition of

fluid domain surrounding the hydrofoil. This fluid domain was designed as a solid part in 3D-CAD and then, the requisite external volume with a cavity of the geometry of the hydrofoil to be examined was obtained. The simulations provided the required information about the velocity and pressure distribution and it should be kept in mind that to obtain good results, one must pay attention to the size of the fluid domain in relation to the size of the geometry that is to be studied [34,25]. The fluid domain must be kept larger so that the flow around the hydrofoil is stable and unaffected by the domain walls [35,26]. Moreover, the 3D-CAD model of the hydrofoil for the CFD simulation included the inflow, outflow, symmetry, and top-bottom boundary conditions, Fig. 13.

##### 4.1. Choice of numerical parameters and solution algorithms

The fluid used in this study is considered an isotropic Newtonian fluid. The initial state of the fluid has been specified as a predefined field. For dynamic incompressible fluid analysis that specifies a turbulence model, initial fluid turbulence values such as vortical viscosity of the vortex should be specified. Fluid properties such as density, initial velocity have also been specified. Table 4 shows the initial properties of the fluid that have been implemented as predefined fields.

##### a. Spalart-Allmaras (SA) turbulence model

In this works, the Spalart-Allmaras (SA) turbulence model is used in Abaqus CFD. This model is a one-equation turbulence model, based on a nonlinear transport equation with the eddy viscosity as a variable. This model is developed mainly for aerodynamics turbulent flows and became a popular due to its accurate results for turbulent flows in industrial complex models. Due to the broad use, the model was even further modified and calibrated for two-dimensional mixing layers, flat-plate boundary layers and wakes. The results of using this model in such turbulent flows with presence of adverse pressure gradients were found accurate, this feature make the Spalart-Allmaras turbulence model applicable for turbulent flows with flow separations. Spalart-Allmaras operates by concerning the various terms in Reynolds stress equation, these terms can be identified in Spalart-Allmaras model as production, diffusion, and destruction of the turbulent eddy; viscosity based on the physics/dynamics of the turbulent flow, when the

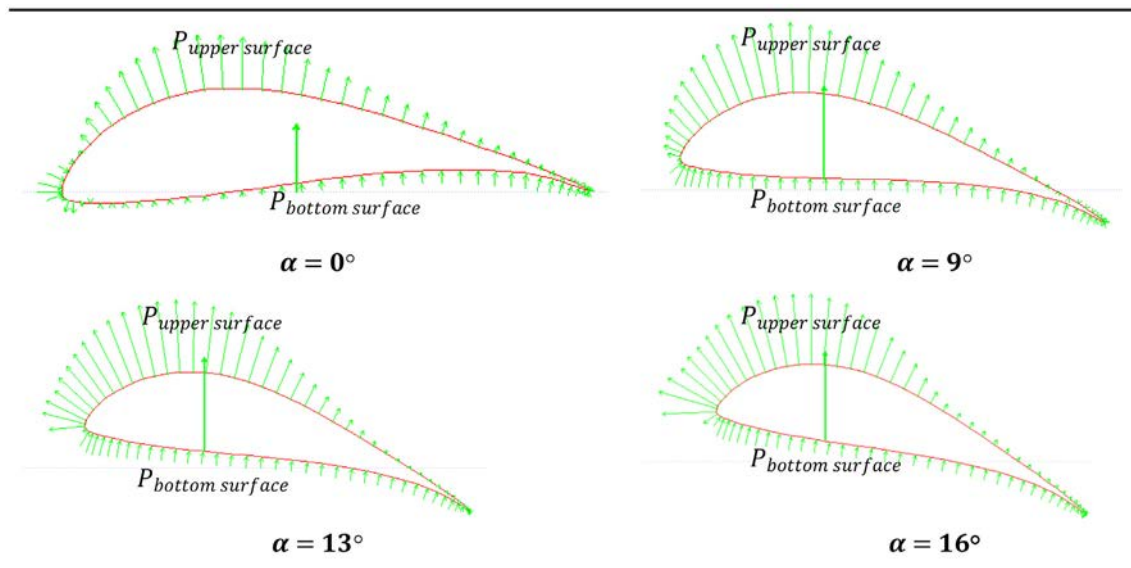
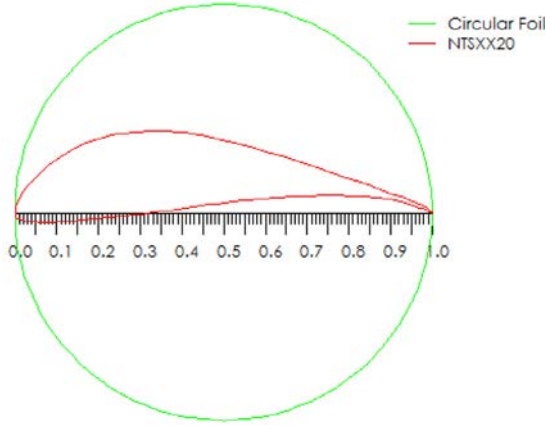
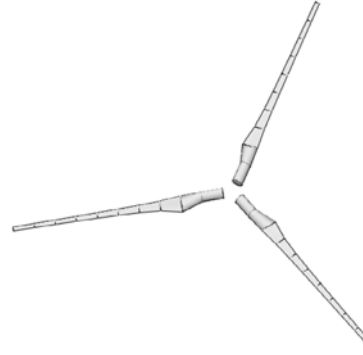


Fig. 10. Schematic representation of lift forces generated in a hydrofoil.



(a) 360° polar Montgomerie



(b) The geometry of the designed rotor

Fig. 11. Design of hydrofoil from the QBlade BEM results.

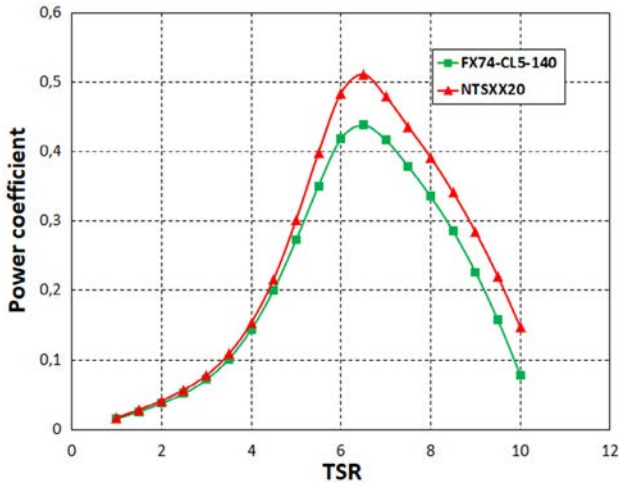


Fig. 12.  $C_{power}$  vs TSR curve from the QBlade BEM results.

kinematic eddy viscosity is the dependent variable and directly related to the Reynolds stress. The differential form of Spalart-Allmaras transport equation is derived by "empiricism and arguments of dimensional analyses, Galilean invariance and selected dependence on the molecular viscosity, see equation (5) [36].

$$\frac{\partial v}{\partial t} + u \frac{\partial v}{\partial x} = C_{b1} S v + \frac{1}{\sigma} \left[ \frac{\partial}{\partial x} \left( \frac{\partial v}{\partial x} (\vartheta + v) + \frac{\partial v}{\partial x} \frac{\partial v}{\partial x} C_{b2} \right) - C_{w1} f_w \left( \frac{v}{d} \right)^2 \right] \quad (5)$$

where:

$v$ : The working variable (turbulent eddy viscosity).

$\vartheta$ : Kinematic eddy viscosity.

$t$ : Time.

$d$ : Normal distance from the wall.

$u$ : Velocity vector.

$x$ : Physical Cartesian coordinate component.

$S$ : Vorticity magnitude.

$f_w$ : Equal to 1 at the interval of the log-layer and decrease at the outer regions.

$C_{b1}$ : Production coefficient equal to (0.1355).

$C_{b2}$ : Cross diffusions coefficient equal to (0.622).

$\sigma$ : Diffusion coefficient of the diffusive transport of the turbulent kinematic eddy viscosity, equal to (2/3).

$C_{w1}$ : Near-wall equilibrium conditions equal to (3.2391).

b. Mesh convergence

Mesh generation is an important step in all finite element analysis cases, including CFD analysis. This step defines the elements or cells that have a significant influence on the calculation and solution of flow field variables, such as velocity, pressure, vorticity, etc. In order to obtain a precise CFD result, the mesh must be carefully generated and well observed.

In order to generate a good mesh quality without the need for a large computing capacity and a large CPU time, the geometry of the fluid domain has been carefully partitioned. The unstructured mesh area has been customized to decrease the amount of elements without affecting the accuracy of the CFD solution, which has been achieved by slightly and successively increasing the length of the elements in the flow direction, which results in a decrease of the quantity of the generated elements and therefore of the required CPU calculation time and of the memory capacity of the computer. Solutions of any finite element analysis must be tested for mesh convergence. This convergence has been tested for 7 mesh size configurations. Fig. 14 shows the size of the elements at each simulation and the value of the velocity at the input (2 m/s). The velocity seems to stabilize around an element size of 0.5–0.6 mm and therefore the solution seems to converge for this value. An element size of 0.5 mm was therefore chosen as the optimal size for a solution independent of the mesh, Fig. 14a. Another way to ensure the convergence of the mesh is to check the RMS error values, Fig. 14b. Lack of verification is a common cause of erroneous results for a CFD calculation, and this process should be performed at least once for each type of problem. In general, one must ensure that the solution meets the following three conditions:

- Residual error values must be reduced to an acceptable value (usually  $10^{-4}$  or  $10^{-5}$ ),
- The control points for our values of interest must reach a stable solution,
- The domain must have imbalances of less than 1%.

The geometry of the fluid domains was neatly remarked to create a good quality mesh with less computational work and time and ABAQUS/CFD enabled the partitioning of the fluid domain into including parts. The geometry was meshed with a four-node

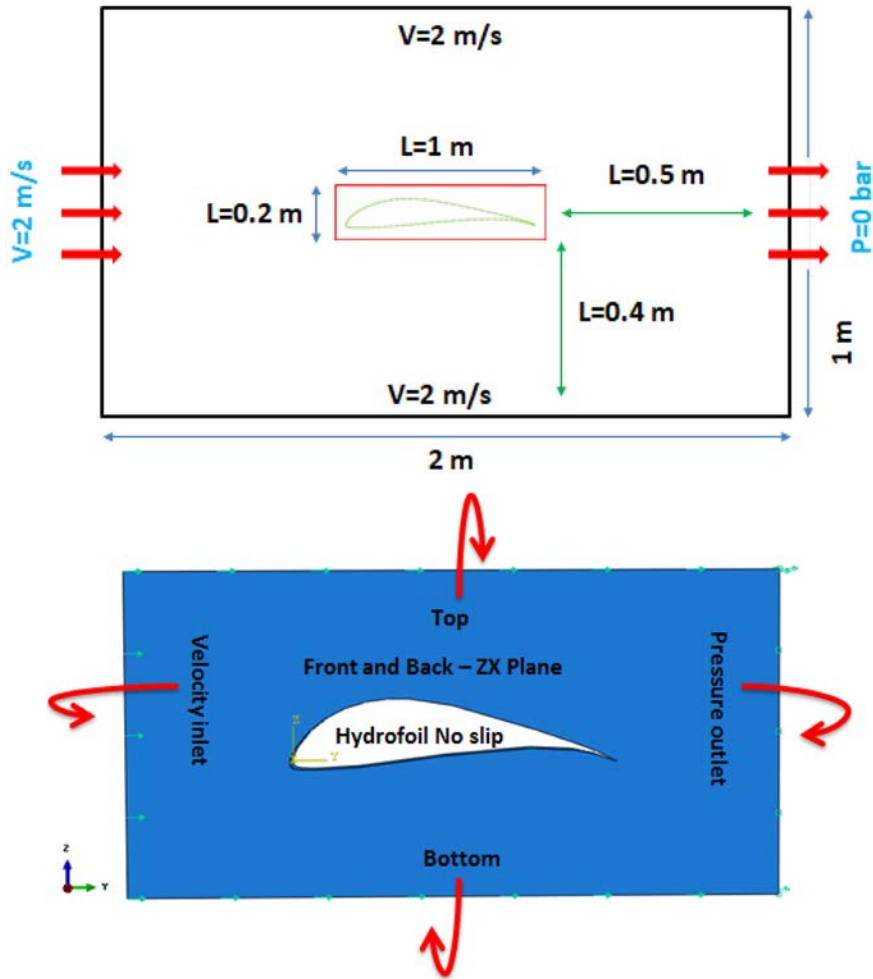


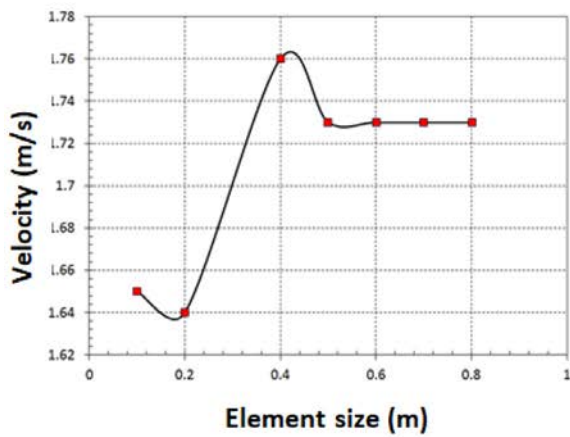
Fig. 13. Schematic diagram of applied boundary conditions in the domain.

Table 4

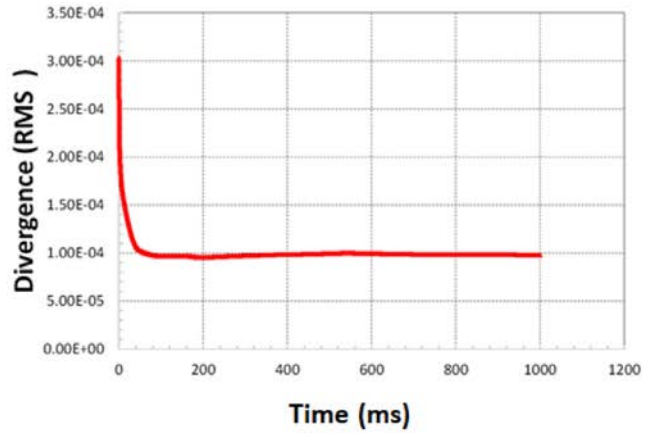
Initial conditions of the fluid.

Kinematic viscosity ( $m^2/s$ )	Density ( $kg/m^3$ )	Dynamic Viscosity (Pa.s)
1.15E-06	1000	0.00115

tetrahedral element (F3D4) then, the simulation domain was meshed for which the physics was defined and solved using regions and limits, Fig. 15.



(a)



(b)

Fig. 14. Mesh convergence.

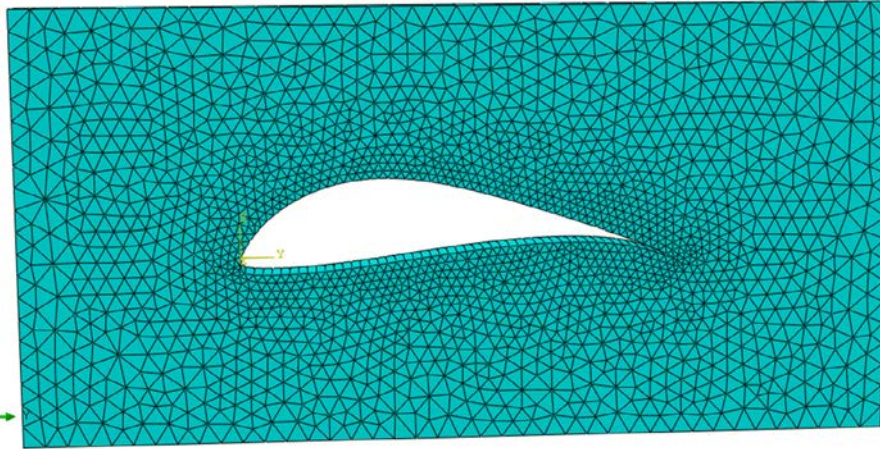


Fig. 15. Mesh geometry.

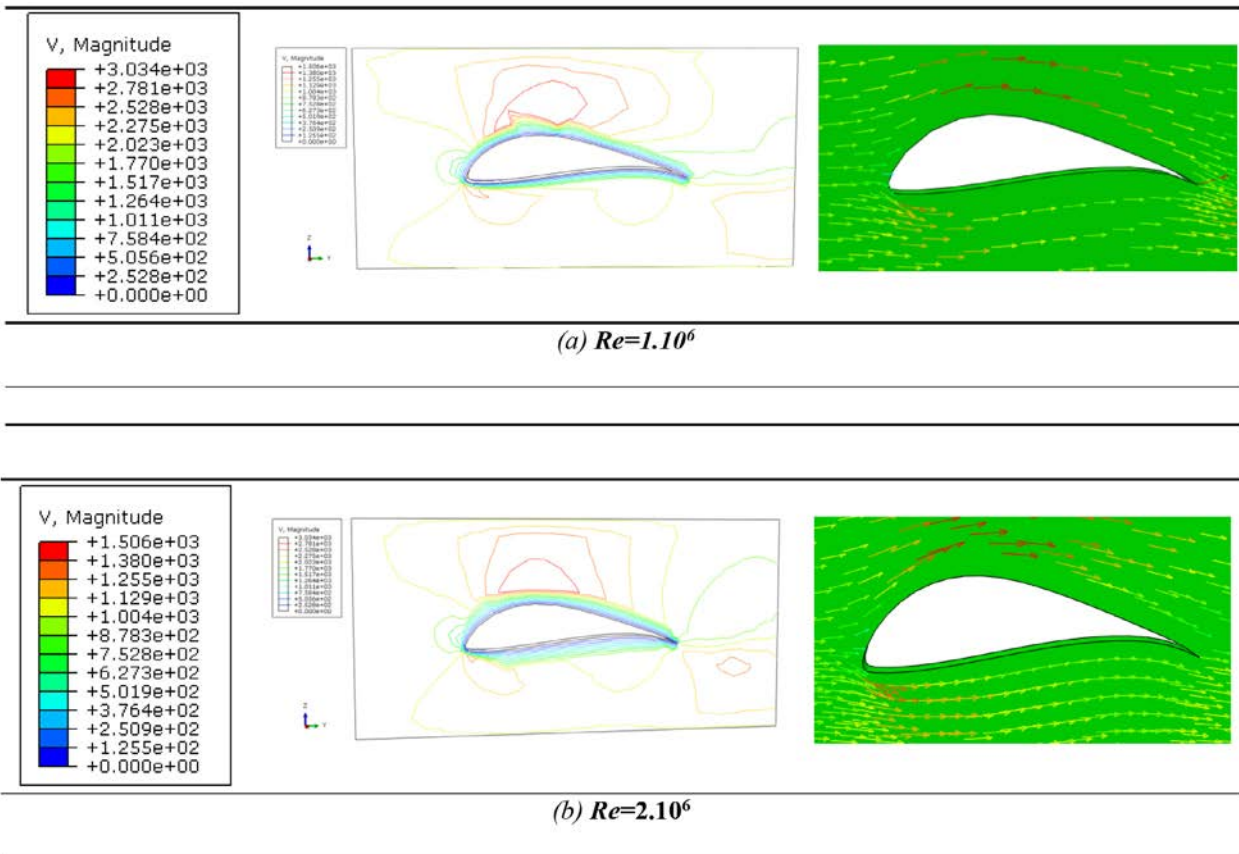


Fig. 16. Velocity distribution (mm/s).

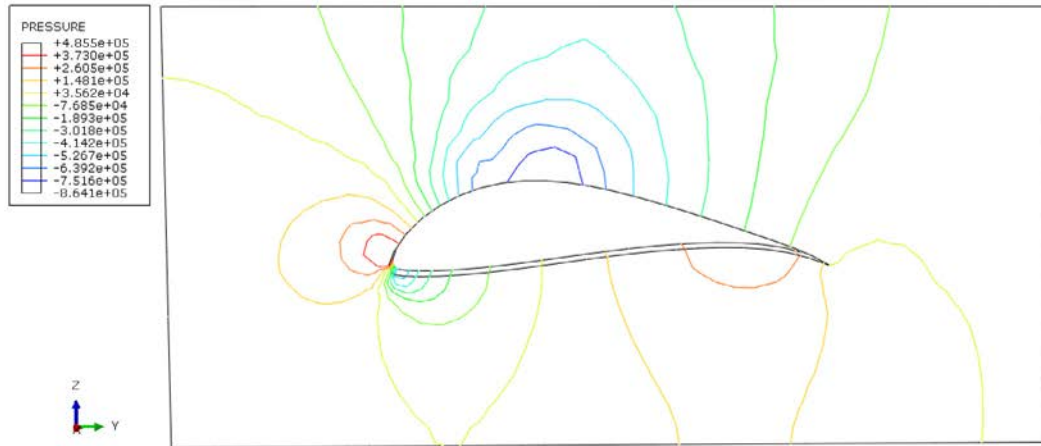
#### 4.2. Results of CFD simulation

Figs. 16 and 17 shows the velocity and pressure distribution for the angle of attack  $\alpha=0^\circ$  and the key factor for extracting energy was the hydrodynamic performance of the hydrofoil. It can clearly be seen that as the velocity of the marine current increases around the leading edge, the result is a pressure drop and a negative pressure inclination. However, as the flow of water advances towards the trailing edge, the velocity decreases and the pressure increases, which ends with the inclination of the positive pressure and consequently the pressure of the water is higher at

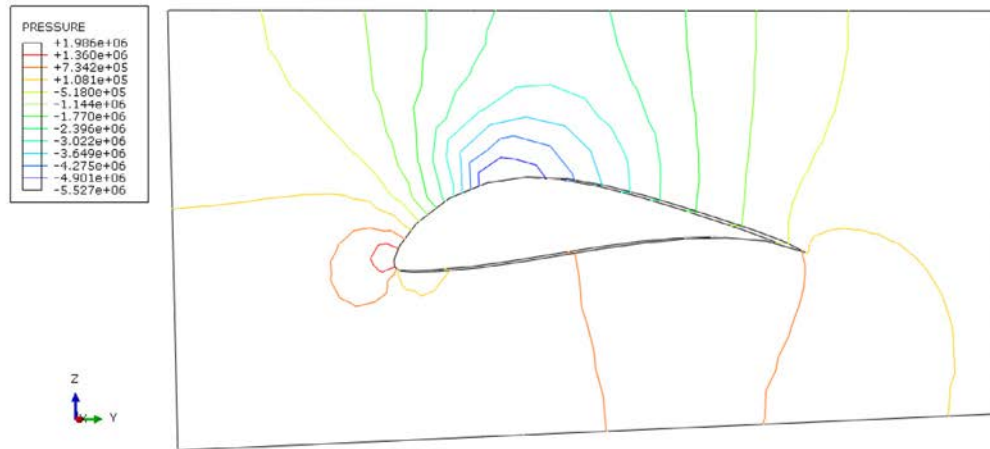
the superior surface and also exceeds the force of gravity that results in the lift force.

#### 5. Conclusions and future development scopes

Tidal current turbine is one of the innovative and emerging technologies of marine renewable energies because it offers constant and predictable energy which can be very useful especially for commercial scale production of electrical power. Hydrofoils (HF) are essential elements of Tidal Current Turbine (TCT) and it



(a)  $Re=1.10^6$



(b)  $Re=2.10^6$

Fig. 17. Pressure distribution (MPa).

must be correctly designed because it plays vital role in improving the turbine output and providing enough resistance to the blade structure. The hydrodynamic performance of a new hydrofoil was studied using XFLR5 and Abaqus/CFD code. As wind Tunnel Test was costly and could not available everywhere, XFLR5 was the excellent tool to analyze and discover out better-suited hydrofoil for a hydrokinetic turbine as per the exigency. In addition, new hydrofoil could be designed and examined according to the requirement at a low price. The Marine current turbine performance curve maintained a  $C_p$  value of over 50% from TSR range of 5 to 9 with maximum  $C_p$  of 51% at  $TSR = 6,5$ .

This work can also provide some support to the industry and academia for the utilization of diverse tidal current energy technologies for reaching a sustainable future. Despite these good results, in future, wind tunnel tests are recommended to endorsed the predictions, particularly for the stall behavior. Moreover, in order to satisfy the requirements of TCTs designs, that are mostly associated with problems such as mass gain, fouling resistance, corrosion resistance, manufacturing methods and coating technology, the future work will involve the use of composite materials because of their excellent mass/durability relations.

### Conflicts of interest

The authors of this paper declare that they have no conflict of interest, and compliance with ethical stand.

### CRediT authorship contribution statement

**M. Nachtane:** Investigation, Data curation, Conceptualization, Writing - original draft, Methodology, Writing - review & editing. **M. Tarfaoui:** Conceptualization, Supervision, Project administration, Software, Resources, Writing - review & editing. **D. Saifaoui:** Supervision, Validation, Conceptualization. **M. Rouway:** Validation, Writing - review & editing.

### Declaration of Competing Interest

The authors declare that they have no known competing financial interests or personal relationships that could have appeared to influence the work reported in this paper.

## References

- [1] D.D.J. Taylor, S. Paiva, A.H. Slocum, An alternative to carbon taxes to finance renewable energy systems and offset hydrocarbon based greenhouse gas emissions, *Sustainable Energy Technol. Assess.* 19 (2017) 136–145, <https://doi.org/10.1016/j.seta.2017.01.003>.
- [2] A. Foley, A.G. Olabi, Renewable energy technology developments, trends and policy implications that can underpin the drive for global climate change, *Renew. Sustain. Energy Rev.* 68 (2017) 1112–1114, <https://doi.org/10.1016/j.rser.2016.12.065>.
- [3] Y. Amry, M. El Gaidi, M. Nachtane, Design and optimization of a smart meter to meet the growing needs of energy in morocco, in: 2016 International Renewable and Sustainable Energy Conference (IRSEC), IEEE, 2016, pp. 1115–1118.
- [4] M. Nachtane, M. Tarfaoui, K. Hilmi, D. Saifaoui, A. El Moumen, Assessment of energy production potential from tidal stream currents in Morocco, *Energies* 11 (2018) 1065, <https://doi.org/10.3390/en11051065>.
- [5] R.H. Charlier, C.W. Finkl, *Ocean Energy: Tide and Tidal Power*, Springer Science & Business Media, 2009.
- [6] Y. Aroussy, M. Nachtane, D. Saifaoui, M. Tarfaoui, Numerical investigation of a reverse osmosis desalination system with cogeneration and renewable energy integration, *Int. J. Sci. Eng. Res.* 7 (2016) 129–133.
- [7] Y. Aroussy, M. Nachtane, D. Saifaoui, M. Tarfaoui, Y. Farah, M. Abid, Using renewable energy for seawater desalination and electricity production in the site OCP Morocco, *J. Sci. Arts* 16 (2016) 395.
- [8] N. Mourad, T. Mostapha, S. Dennoun, Promotion of renewable marines energies in Morocco: perspectives and strategies, *World Acad. Sci. Eng. Technol. Int. J. Energy Power Eng.* 12 (2018).
- [9] M. Tarfaoui, M. Nachtane, H. Boudounit, Finite element analysis of composite offshore wind turbine blades under operating conditions, *J. Thermal Sci. Eng. Appl.* 12 (2020), <https://doi.org/10.1115/1.4042123>.
- [10] M. Tarfaoui, O.R. Shah, M. Nachtane, Design and optimization of composite offshore wind turbine blades, *J. Energy Resour. Technol.* 141 (2019), <https://doi.org/10.1115/1.4042414>.
- [11] S. Griffiths, A review and assessment of energy policy in the Middle East and North Africa region, *Energy Policy* 102 (2017) 249–269, <https://doi.org/10.1016/j.enpol.2016.12.023>.
- [12] R.H. Charlier, A “sleeper” awakes: tidal current power, *Renew. Sustain. Energy Rev.* 7 (2003) 515–529, [https://doi.org/10.1016/S1364-0321\(03\)00079-0](https://doi.org/10.1016/S1364-0321(03)00079-0).
- [13] M. Tarfaoui, A. El Moumen, K. Lafdi, O. Hassoon, M. Nachtane, Inter laminar failure behavior in laminate carbon nanotubes-based polymer composites, *J. Compos. Mater.* 52 (2018) 3655–3667, <https://doi.org/10.1177/0021998318767493>.
- [14] M. Tarfaoui, M. Nachtane, A. El Moumen, Energy dissipation of stitched and unstitched woven composite materials during dynamic compression test, *Compos. B Eng.* 167 (2019) 487–496.
- [15] O.H. Hassoon, M. Tarfaoui, A. El Moumen, Y. Qureshi, H. Benyahia, M. Nachtane, Mechanical performance evaluation of sandwich panels exposed to slamming impacts: comparison between experimental and SPH results, *Compos. Struct.* 220 (2019) 776–783.
- [16] M. Nachtane, M. Tarfaoui, S. Sassi, A. El Moumen, D. Saifaoui, An investigation of hydrothermal aging effects on high strain rate behaviour of adhesively bonded composite joints, *Compos. B Eng.* 172 (2019) 111–120, <https://doi.org/10.1016/j.compositesb.2019.05.030>.
- [17] S. Sassi, M. Tarfaoui, M. Nachtane, Yahia H. Ben, Strain rate effects on the dynamic compressive response and the failure behavior of polyester matrix, *Compos. B Eng.* 174 (2019), <https://doi.org/10.1016/j.compositesb.2019.107040>.
- [18] M.R. Ahmed, Blade sections for wind turbine and tidal current turbine applications—current status and future challenges, *Int. J. Energy Res.* 36 (2012) 829–844, <https://doi.org/10.1002/er.2912>.
- [19] J.N. Goundar, M.R. Ahmed, Design of a horizontal axis tidal current turbine, *Appl. Energy* 111 (2013) 161–174, <https://doi.org/10.1016/j.apenergy.2013.04.064>.
- [20] M.J. Lawson, Y. Li, D.C. Sale, Development and Verification of a Computational Fluid Dynamics Model of a Horizontal-Axis Tidal Current Turbine, American Society of Mechanical Engineers Digital Collection, 2011, pp. 711–720, <https://doi.org/10.1115/OMAE2011-49863>.
- [21] F. Grasso, Design and optimization of tidal turbine airfoil, *J. Aircraft* 49 (2012) 636–643, <https://doi.org/10.2514/1.C031617>.
- [22] W.M.J. Batten, A.S. Bahaj, A.F. Molland, J.R. Chaplin, The prediction of the hydrodynamic performance of marine current turbines, *Renewable Energy* 33 (2008) 1085–1096, <https://doi.org/10.1016/j.renene.2007.05.043>.
- [23] A.F. Molland, A.S. Bahaj, J.R. Chaplin, W.M.J. Batten, Measurements and predictions of forces, pressures and cavitation on 2-D sections suitable for marine current turbines, *Proc. Inst. Mech. Eng., M* 218 (2004) 127–138, <https://doi.org/10.1243/1475090041651412>.
- [24] M. Nachtane, M. Tarfaoui, A. El Moumen, D. Saifaoui, Numerical investigation of damage progressive in composite tidal turbine for renewable marine energy, in: 2016 International Renewable and Sustainable Energy Conference (IRSEC), 2016, pp. 559–563, <https://doi.org/10.1109/IRSEC.2016.7984026>.
- [25] M. Nachtane, M. Tarfaoui, D. Saifaoui, Matériaux composites pour les énergies marines renouvelables, Éditions universitaires européennes, 2017.
- [26] O.H. Hassoon, M. Tarfaoui, A. El Moumen, H. Benyahia, M. Nachtane, Numerical evaluation of dynamic response for flexible composite structures under slamming impact for naval applications, *Appl. Compos. Mater.* 25 (2018) 689–706, <https://doi.org/10.1007/s10443-017-9646-0>.
- [27] M. Tarfaoui, M. Nachtane, H. Khadimallah, D. Saifaoui, Simulation of mechanical behavior and damage of a large composite wind turbine blade under critical loads, *Appl. Compos. Mater.* 25 (2018) 237–254, <https://doi.org/10.1007/s10443-017-9612-x>.
- [28] W. Li, H. Zhou, H. Liu, Y. Lin, Q. Xu, Review on the blade design technologies of tidal current turbine, *Renew. Sustain. Energy Rev.* 63 (2016) 414–422, <https://doi.org/10.1016/j.rser.2016.05.017>.
- [29] M. Nachtane, M. Tarfaoui, A. El Moumen, D. Saifaoui, Damage prediction of horizontal axis marine current turbines under hydrodynamic, hydrostatic and impacts loads, *Compos. Struct.* 170 (2017) 146–157, <https://doi.org/10.1016/j.compstruct.2017.03.015>.
- [30] J.N. Goundar, M.R. Ahmed, Y.-H. Lee, Numerical and experimental studies on hydrofoils for marine current turbines, *Renewable Energy* 42 (2012) 173–179, <https://doi.org/10.1016/j.renene.2011.07.048>.
- [31] S.A. Oller Aramayo, L.G. Nallim, S.H. Oller Martínez, The usability of the Selig S1223 profile airfoil as a high lift hydrofoil for hydrokinetic application, *J. Appl. Fluid Mech.* 9 (2016) 537–542.
- [32] R. Balaka, A. Rachman, Pitch angle effect for horizontal axis river current turbine, *Procedia Eng.* 50 (2012) 343–353.
- [33] W.M.J. Batten, A.S. Bahaj, A.F. Molland, J.R. Chaplin, Hydrodynamics of marine current turbines, *Renewable Energy* 31 (2006) 249–256, <https://doi.org/10.1016/j.renene.2005.08.020>.
- [34] T. Xing, J. Shao, F. Stern, BKW-RS-DES of unsteady vortical flow for KVLCC2 at large drift angles, in: Proc 9th Int Conf on Numerical Ship Hydrodynamics, Ann Arbor, MI, 2007, pp. 5–8.
- [35] X.-Z. Chen, D.-P. Shi, X. Gao, Z.-H. Luo, A fundamental CFD study of the gas-solid flow field in fluidized bed polymerization reactors, *Powder Technol.* 205 (2011) 276–288, <https://doi.org/10.1016/j.powtec.2010.09.039>.
- [36] M. Nachtane, M. Tarfaoui, A.E. Moumen, D. Saifaoui, H. Benyahia, Design and hydrodynamic performance of a horizontal axis hydrokinetic turbine, *Int. J. Automotive Mech. Eng.* 16 (2019) 6453–6469, <https://doi.org/10.15282/ijame.16.2.2019.1.0488>.